The Journal of Chemical Physics ARTICLE scitation.org/journal/jcp

High-resolution infrared spectroscopy of supersonically cooled singlet carbenes: Bromomethylene (HCBr) in the CH stretch region

Cite as: J. Chem. Phys. 156, 014304 (2022); doi: 10.1063/5.0077341
Submitted: 1 November 2021 • Accepted: 5 December 2021 •
Published Online: 4 January 2022

Ya-Chu Chan,[1,2] Andrew Kortyna,[3] and David J. Nesbitt[1,2,4,a)]

AFFILIATIONS

[1] JILA, University of Colorado Boulder and National Institute of Standards and Technology, Boulder, Colorado 80309, USA
[2] Department of Chemistry, University of Colorado Boulder, Boulder, Colorado 80309, USA
[3] Cold Quanta, 3030 Sterling Circle, Boulder, Colorado 80301, USA
[4] Department of Physics, University of Colorado Boulder, Boulder, Colorado 80309, USA

[a)] Author to whom correspondence should be addressed: djn@jila.colorado.edu

ABSTRACT

First high-resolution spectra of cold (~35 K) singlet bromomethylene HCBr in the CH stretching (v_1) region from 2770 to 2850 cm^{-1} are reported using near quantum shot-noise limited laser absorption methods in a slit jet supersonic discharge expansion source. Three rovibrational bands are identified at high S/N (20:1–40:1) and rotationally assigned to (i) the CH stretch fundamental (v_1) band $\tilde{X}(1,0,0) \leftarrow \tilde{X}(0,0,0)$ and (ii) vibrational hot bands [$\tilde{X}(1,1,0) \leftarrow \tilde{X}(0,1,0)$ and $\tilde{X}(1,0,1) \leftarrow \tilde{X}(0,0,1)$] arising from vibrationally excited HCBr populated in the discharge with single quanta in either the H–C–Br bend (v_2) or C–Br stretch (v_3) modes. Precision rotational constants are reported for a total of six states, with an experimentally determined CH stretch vibrational frequency (2799.38 cm^{-1}) in good agreement with previous low-resolution fluorescence studies [M. Deselnicu *et al.*, J. Chem. Phys. **124**(13), 134302 (2006)]. Detailed analysis of the fundamental v_1 band highlights the presence of perturbations in the $\tilde{X}(1,0,0)$ level, which we tentatively attribute to arise from the nearby triplet state $\tilde{a}(0,0,1)$ through spin–orbit interaction or the multiple quanta $\tilde{X}(0,2,1)$ singlet state via c-type Coriolis coupling. Reduced-Doppler resolution (60 MHz) in the slit-jet IR spectrometer permits for clear observation of a nuclear spin hyperfine structure, with experimental line shapes well reproduced by nuclear quadrupole/spin-rotation coupling constants from microwave studies [C. Duan *et al.*, J. Mol. Spectrosc. **220**(1), 113–121 (2003)]. Finally, the a-type to b-type transition intensity ratio for the fundamental CH stretch band is notably larger than that predicted by using a bond-dipole model, which from high level *ab initio* quantum calculations [CCSD(T)/PVQZ] can be attributed to vibrationally induced "charge-sloshing" of electron density along the polar C–Br bond.

Published by AIP Publishing. https://doi.org/10.1063/5.0077341

I. INTRODUCTION

Carbenes (:CR_1R_2) are transient reactive intermediates that play key roles in a variety of chemical reactions.[1–3] Although reactions with these species were initially misdescribed as "indiscriminate" in the 1960s,[4,5] carbenes are now known to facilitate highly selective synthetic methodologies widely used in organic chemistry and with important applications in industrial synthesis.[6–9] Due to the presence of two non-bonding electrons, carbenes can be in either singlet (spin-paired) or triplet (biradical) states, with distinct chemical reactivities arising from differences in the electronic configuration.[10] In order to understand the chemistry of carbenes, accurate knowledge of substituent effects (R_1, R_2) on the reactivity, ground state multiplicity, and the singlet–triplet energy gap (ΔE_{ST}) is essential. As the prototypical carbene, methylene has a triplet ground state ($^3CH_2$) and has been the target of extensive investigation.[11–14] Indeed, this has served as a textbook example for the synergism between experiment and theory in quantitatively unraveling the detailed properties of this deceptively "simple" triatomic molecule. By way of contrast, the mono- and

di-halocarbenes (:CXY, X = H, F, Cl, Br, and I and Y = F, Cl, Br, and I) represent carbenes with a singlet ground state, though they have also received considerable attention.[15]

Spectroscopic interest in mono-halocarbenes stems from the three low-lying electronic states ($\tilde{X}^1A'$, $\tilde{a}^3A''$, and $\tilde{A}^1A''$),[15] where the two singlet states form a Renner–Teller pair that becomes the doubly degenerate $^1\Delta$ state for a linear configuration.[16] Excitation in the optically allowed $\tilde{A}^1A'' \leftarrow \tilde{X}^1A'$ electronic systems for HCF,[17,18] HCCl,[19] HCBr,[20] and HCI[21] has been investigated by several groups using laser-induced fluorescence (LIF) and near-infrared (NIR) absorption spectroscopy. The triplet state $\tilde{a}^3A''$ is nearly isoenergetic with the singlet ground state $\tilde{X}^1A'$ manifold and, depending on relative energies between electronic manifolds, can mix with either the singlet ground state ($\tilde{X}^1A'$) or the the singlet ground ($\tilde{X}^1A'$) or excited ($\tilde{A}^1A''$) states via resonant spin–orbit interactions.[22] Such mixing behavior was, in fact, reported by Butcher *et al.* for localized singlet–triplet crossings between the $\tilde{A}^1A''$ and $\tilde{a}^3A''$ states in Zeeman spectra of HCF,[23] where the singlet–triplet energy gap is comparatively large [ΔE_{ST} = 62.3(17) kJ/mol[24]]. For the heavier HCCl,[25,26] HCBr,[27–29] and HCI[21] species, on the other hand, the singlet–triplet energy gaps are now small enough such that global spin–orbit interactions with $\tilde{a}^3A''$ states can be probed by global shifts/perturbations in rovibrationally excited levels of the singlet ground $\tilde{X}^1A'$ electronic state. Indeed, Chang and co-workers and Reid and co-workers both report the identification and assignment of triplet vibronic levels in dispersed fluorescence spectra and single vibronic level (SVL) emission spectra due to intensity borrowing from nearby singlet states.[25,27,28] Nevertheless, rotationally resolved spectra of transitions to the triplet-perturbed singlet states or even pure singlet–triplet transitions, which enable detailed analysis of spin–orbit coupling and yield information on the triplet structure, have been obtained only for HCCl via stimulated emission pumping (SEP) spectroscopy.[30] However, explicit rotational state crossings between the triplet and singlet rovibrational energy manifolds were not observed, and thus, the vibronic spin–orbit matrix elements were inferred from the vibrational state dependence for spin–spin parameters in the triplet $\tilde{a}^3A''$ state.

With a singlet–triplet energy gap [ΔE_{ST} = 2006(2) cm^{-1}] comparable to its vibrational mode spacings,[27] bromomethylene (HCBr) represents a quintessential target for the high resolution infrared study of spin–orbit interaction between the singlet ground state $\tilde{X}^1A'$ and triplet excited state $\tilde{a}^3A''$. The three vibrational modes of this bent triatomic in the ground electronic state (Fig. 1) are the CH stretch (v_1) at 2802(2) cm^{-1}, the HCBr bend (v_2) at 1119(2) cm^{-1}, and the CBr stretch (v_3) at 677(2) cm^{-1}.[27] In addition, Duan *et al.* reported the pure rotational microwave spectrum of singlet bromomethylene, providing precise determination of rotational, centrifugal distortion, and ^{79,81}Br nuclear quadrupole and spin-rotation coupling constants for the ground vibrational state.[31] For the vibrationally excited states, Sears and co-workers presented high-resolution rovibronic spectra for hot bands in the $\tilde{A}^1A'' \leftarrow \tilde{X}^1A'$ Renner–Teller pair systems,[32,33] from which the rotational constants of the $\tilde{X}(0,0,1)$, $\tilde{X}(0,1,0)$, and $\tilde{X}(0,2,0)$ levels can be determined. From analysis of the v_2 bending vibration level structure, they identified the presence of a homogeneous perturbation in the $\tilde{X}(0,2,0)$ state (band origin at ~2310 cm^{-1}), plausibly arising from interactions with the zero-point level in the triplet state. Due to weak Franck–Condon factors, however, transitions to/from $\tilde{X}(1,0,0)$ were unfortunately below the detection limit, and thus, the rovibrational structure for this manifold has remained unidentified. It is worth noting that the "dark" $\tilde{a}(0,0,1)$ triplet state [band origin at 2741(2) cm^{-1}] was observed in the emission spectra,[27] with transition intensity possibly arising from the spin–orbit mixing and therefore intensity borrowing from the nearby "bright" $\tilde{X}(1,0,0)$ state. As a result, rotationally resolved infrared spectra for the $\tilde{X}(1,0,0)$ state could provide invaluable information on spin–orbit interaction between the singlet and triplet state manifolds.

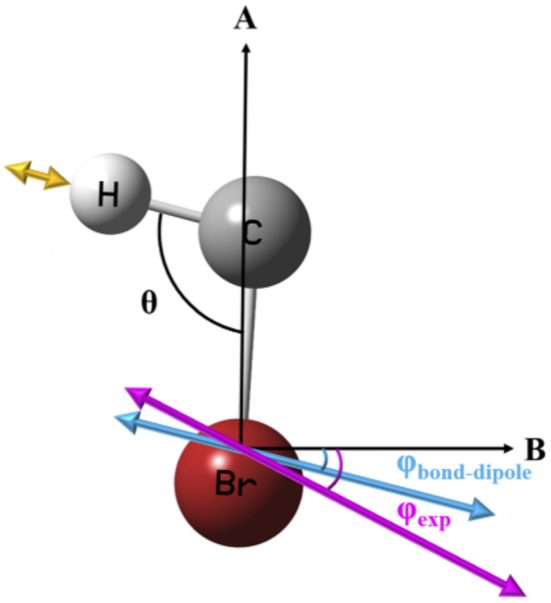

FIG. 1. The HCBr CCSD(T)/cc-pVQZ equilibrium structure and vibrational motion of the (1,0,0) CH stretch mode (yellow arrow). The molecule lies in the plane of the principal rotation axes A and B, whereas the C axis, with the largest moment of inertia, is directed into the page. θ is the H–C–Br bond angle, $\phi_{\text{bond-dipole}}$ is the theoretical angle between the B axis and the CH transition moment from a bond-dipole model [$(\partial\mu/\partial Q)_{\text{bond-dipole}}$, blue arrow], and ϕ_{exp} is the corresponding angle between the B axis and the experimentally determined CH transition dipole moment direction [$(\partial\mu/\partial Q)_{\text{exp}}$, pink arrow].

In this work, first high-resolution, fully rotationally resolved absorption spectra of singlet bromomethylene HCBr in the mid-infrared region (2770–2850 cm^{-1}) are reported. A total of three rovibrational bands are observed, with one being the fundamental C–H stretch band $\tilde{X}(1,0,0) \leftarrow \tilde{X}(0,0,0)$, and the other two being the hot bands from vibrationally exited states, $\tilde{X}(1,1,0) \leftarrow \tilde{X}(0,1,0)$ and $\tilde{X}(1,0,1) \leftarrow \tilde{X}(0,0,1)$. The organization of this paper is as follows. In Sec. II, the experimental approach is briefly described, with experimental spectra presented in Sec. III and spectral analysis yielding precision spectroscopic constants for the $\tilde{X}(0,0,0)$, $\tilde{X}(0,0,1)$, $\tilde{X}(0,1,0)$, $\tilde{X}(1,0,0)$, $\tilde{X}(1,0,1)$, and $\tilde{X}(1,1,0)$ vibrational states of the two common bromine isotopologues. Broadening due to the partially resolved hyperfine structure from ^{79,81}Br nuclear spin is analyzed in Sec. IV A, and determination of the body fixed transition moment $\partial\boldsymbol{\mu}/\partial Q$ and enhancement of a- vs b-type transition intensities due to vibrationally induced "charge-sloshing" effects are

shown in Sec. IV B. In addition, Boltzmann analysis of the two hot bands (Sec. IV C) reveals distinctly non-equilibrium vibrational distributions among the HCBr bending (v_2) and CBr stretching vibrational modes (v_3), which provide insights into vibrational excitation/relaxation pathways in the slit jet discharge expansion source. Finally, extensive rovibrational progressions of CH $\tilde{X}^2\Pi\, v = 1 \leftarrow 0$ are found in this spectral region, with the discharge current dependence of HCBr and CH radical concentrations analyzed in the context of a simple kinetic model (as described in the supplementary material).

II. EXPERIMENT

The supersonic slit-jet discharge IR absorption spectrometer has been described elsewhere in detail.[34] Briefly, a negative polarity 50 kHz square wave electric field of −8400 V/cm is applied between the slit electrodes and valve body, generating peak discharge currents of ~250 mA. The HCBr radicals are produced in the pulsed discharge beam source by coflowing 0.35% bromoform ($CHBr_3$) in a mixture of Ne (59%), He (25%), and H_2 (16%) with a 390 mbar backing pressure in the stagnation region. The $HCBr_2$–Br bond enthalpy, HCBr–Br bond enthalpy, and electron affinity of the Br atom are known to be 267, 273, and −324.6(3) kJ/mol,[35,36] respectively. Thus, precursor molecules and radicals in the discharge region can undergo exothermic dissociative electron attachment to generate HCBr radicals, i.e., $CHBr_3 + e^- \rightarrow HCBr_2 + Br^-$ and $HCBr_2 + e^- \rightarrow HCBr + Br^-$ (see the supplementary material for analysis via one simple kinetic model). Since the HCBr absorption signals are empirically enhanced by the presence of H_2 in the carrier gas, we can presume that the formation of HCBr radicals is also assisted by H atom chemistry. The resulting HCBr radicals are then supersonically expanded through a 300 μm × 4 cm slit operating at a repetition rate of 19 Hz and with a 1 ms pulse width. This isentropic slit expansion cools the initially hot radicals to 35 K, enhancing population density in the lower energy rotational levels and minimizing spectral congestion.

A tunable ring dye laser (Spectra-Physics 380A, R6G dye) and a fixed frequency Ar^+ laser (Spectra-Physics Series 2000, 514.5 nm), both operating on a single mode, are mixed in a periodically poled MgO:$LiNbO_3$ crystal (MgO:PPLN) to generate mid-IR light (5–10 μW, tunable from 2600 to 3450 cm^{-1}) via difference-frequency generation. Precise temperature control of the PPLN crystal ensures quasi-phase matching condition to be met for the difference-frequency component. The Ar^+ laser is locked to a 250 MHz optical transfer cavity locked to a polarization-stabilized HeNe laser,[37] while the ring dye laser is locked to a scanning Fabry–Pérot cavity, achieving narrow-band operation of a few MHz rms for the difference frequency IR radiation. This IR light is split into a reference beam and a signal beam, the latter of which is directed into a 16-pass Herriott cell (64 cm absorption path length) in the vacuum chamber and travels parallel to the 4 cm slit jet axis 2–5 mm downstream of the discharge orifice, with the reference and signal beams focused onto balanced liquid nitrogen cooled InSb detectors in order to facilitate subtraction of common mode technical laser noise. The 50 kHz discharge-modulated radical absorption signal is analyzed by phase-sensitive lock-in detection with a time constant of 100 μs. The spectrum is recorded with a total integration time of 8 ms per frequency point (i.e., 8 gas pulse average) and a 12.5 MHz step between points. For the K_a: 2 ← 1 subband (weaker due to reduced Boltzmann population in K_a = 1), the final spectrum is obtained by averaging three spectral scans (each with an integration time of 10 ms per point and a frequency step of 7.5 MHz) in order to permit better resolution of spectral structure/broadening caused by the Br atom nuclear spin effects. Scans are performed in triplicate to most efficiently determine center frequencies and uncertainties for individual transitions. For 50 kHz slit discharge modulation of radicals and high-bandwidth (10 MHz) subtraction of the technical laser noise, a root-mean-square absorbance noise of 2.2×10^{-6} $Hz^{-1/2}$ is routinely obtained, yielding an experimental signal-to-noise ratio of ~67 for the strongest HCBr $K_a = 1 \leftarrow 0$ Q-branch signals. By linear interpolation between dye laser transmission fringes through the stabilized optical transfer cavity, relative frequencies at the sub-10 MHz precision level are achieved. The spectrometer is calibrated daily against four rovibrational lines in the CH_4 ν_3 P(4) manifold,[38] yielding results with ±11 MHz frequency accuracy. The instrumental reduced-Doppler linewidths are limited to ~60 MHz (0.002 cm^{-1}) due to the minor non-orthogonal Herriott cell crossings ($\Delta\theta \approx 12°$) between the difference frequency IR laser and the slit expansion velocity. However, the observed rovibrational lines are also broadened due to nuclear spin hyperfine effects of the Br atom (I_{Br} = 3/2), resulting in average experimental linewidths of 96 MHz (0.0032 cm^{-1}).

III. EXPERIMENTAL SPECTRUM AND ANALYSIS

A. Fundamental band $\tilde{X}(1,0,0) \leftarrow \tilde{X}(0,0,0)$

High-resolution IR absorption spectra of jet-cooled singlet bromomethylene radicals HCBr have been multiply recorded in the CH stretch region from 2770 to 2850 cm^{-1}. HCBr is a bent, triatomic molecule, with the direction of the CH stretch transition dipole moment lying in the molecular plane and between the a- and b-axes (Fig. 1). Therefore, one expects to observe both a-type (ΔK_a = even, ΔK_c = odd) and b-type (ΔK_a = odd, ΔK_c = odd) transitions in the CH stretch fundamental rovibrational band of HCBr. Figure 2(a) displays Q-branches for the three observed b-type K_a-subbands, where the obvious doublet structure originates from the two stable isotopes of the bromine atom, ^{79}Br and ^{81}Br, present in nearly equal natural isotopic abundances (51%:49%). Since the CH stretch band origin of H^{79}Br is slightly shifted to the blue while its rotational constants are larger compared to H^{81}Br, several overlapping and crossover features in the Q-branches are observed in the corresponding K_a: 0 ← 1 subband. In the K_a: 2 ← 1 subband, the $J_{2,J-2} \leftarrow J_{1,J-1}$ Q-branch transition intensities are reduced from the $J_{2,J-1} \leftarrow J_{1,J-2}$ Q-branch, while the integrated intensities are the same for the two Q-branches. This is due to nuclear spin broadening by the Br atom, as discussed in more detail in Sec. IV A. The HCBr a-type transitions are shown in Fig. S1, where P- and R-branches of the K_a: 0 ← 0, K_a: 1 ← 1, and K_a: 2 ← 2 subbands are observed. Complete lists of rotationally assigned a- and b-type transitions in the $\tilde{X}(1,0,0) \leftarrow \tilde{X}(0,0,0)$ band are provided in the supplementary material (Tables S1 and S2).

The PGOPHER simulations[39] of the $\tilde{X}(1,0,0) \leftarrow \tilde{X}(0,0,0)$ band in Figs. 2(a) and S1 are described by an A-reduced Watson non-rigid asymmetric top Hamiltonian in the I^r representation,[40]

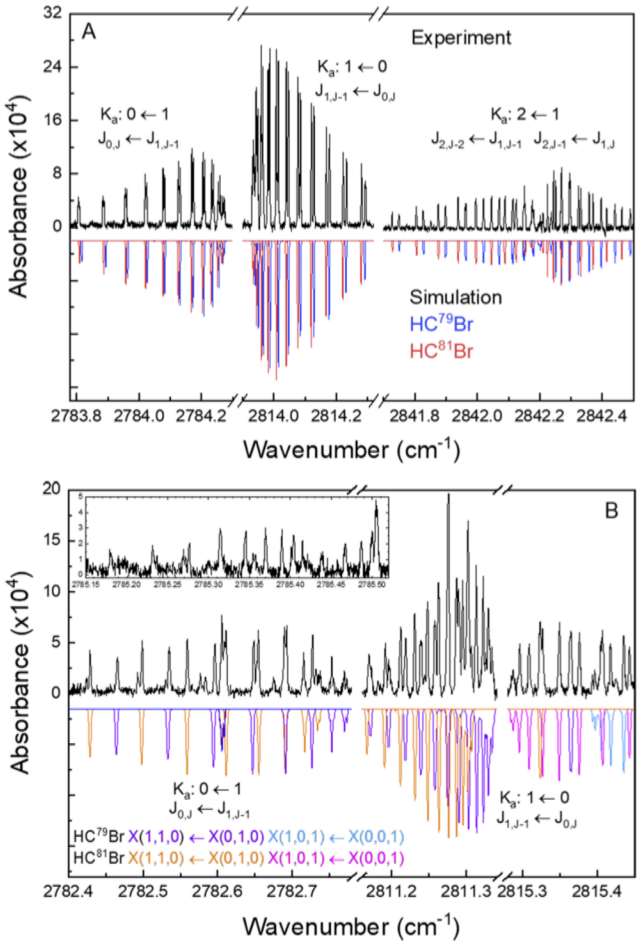

FIG. 2. (a) The experimental absorption spectrum of the HCBr $\tilde{X}(1,0,0) \leftarrow \tilde{X}(0,0,0)$ band (black), showing Q-branches of K_a: 0 ← 1, K_a: 1 ← 0, and K_a: 2 ← 1 subbands. Spectral simulation using PGOPHER assumes a rotational temperature of 35 K (see Boltzmann analysis in Sec. IV B) and Gaussian linewidths of 60 MHz. The upper state spectroscopic constants used in the simulation are from the fit including the quartic centrifugal distortion constant Δ_J', Δ_{JK}', and Δ_K'. The effects of nuclear spin in HCBr are evidenced by broadening and splitting of the lines (see Fig. 3 for the detailed partially resolved hyperfine structure in the K_a: 2 ← 1 Q-branch). (b) Part of the Q-branches of the $\tilde{X}(1,0,1) \leftarrow \tilde{X}(0,0,1)$ and $\tilde{X}(1,1,0) \leftarrow \tilde{X}(0,1,0)$ hot bands of HCBr. For $HC^{79}Br$, the PGOPHER simulations of the $\tilde{X}(1,0,1) \leftarrow \tilde{X}(0,0,1)$ and $\tilde{X}(1,1,0) \leftarrow \tilde{X}(0,1,0)$ transitions are shown in light blue and purple, respectively. For $HC^{81}Br$, the transitions of the two bands are shown in magenta and orange. The inset displays the Q-branch region of the $\tilde{X}(1,0,1) \leftarrow \tilde{X}(0,0,1)$ K_a: 0 ← 1 subband, although definitive rotational assignments have not been made.

$$\hat{H}_{rot} = A\hat{J}_z^2 + B\hat{J}_x^2 + C\hat{J}_y^2 - \Delta_J\hat{J}^4 - \Delta_{JK}\hat{J}^2\hat{J}_z^2 - \Delta_K\hat{J}_z^4 - \frac{1}{2}\left[\delta_J\hat{J}^2 + \delta_K\hat{J}_z^2, \hat{J}_+^2 + \hat{J}_-^2\right]_+ + \Phi_J\hat{J}^6 + \Phi_{KJ}\hat{J}^2\hat{J}_z^4. \quad (1)$$

The ground state rotational and centrifugal distortion constants used in the simulations are obtained from combined least squares fits to (i) ground state combination differences of the $\tilde{X}(1,0,0) \leftarrow \tilde{X}(0,0,0)$ transitions in this work and (ii) hyperfine-resolved pure rotational lines in the previous kinetic microwave spectroscopic work by Duan *et al.*[31] To avoid degraded precision in the hyperfine-resolved microwave data, each hyperfine-free $\tilde{X}(1,0,0) \leftarrow \tilde{X}(0,0,0)$ transition in this work is represented by a weighted average of its hyperfine components. The combined least squares fits are furthermore weighted by $\frac{1}{\sigma_i^2}$, where σ_i is the standard uncertainty of the observed transition. The resulting HCBr ground state spectroscopic constants are summarized in Table I. By way of comparison, the microwave data by Duan *et al.* are also re-fitted using the PGOPHER program, with the ground state rotational, centrifugal distortion, and Br atom nuclear spin constants reported. Uncertainties in the combined IR/microwave fits are now reduced by as much as 17-fold compared to the microwave work, as a result of greatly reduced parameter correlation between A and Δ_K due to both a- and b-type transitions in the dataset. Interestingly, these improved ground state constants for both $HC^{79}Br$ and $HC^{81}Br$ are, nevertheless, still in respectably good agreement (i.e., within 3σ) with the microwave results.

Table II presents a summary of the observed vibrationally excited state constants for $HC^{79}Br$ and $HC^{81}Br$. In order to break parameter correlation and best characterize the $\tilde{X}(1,0,0)$ state, the ground state rotational constants in the least squares fits have been held fixed at the $\tilde{X}(0,0,0)$ values reported in Table I. Of particular relevance, the results reveal that a standard asymmetric top Watson Hamiltonian cannot provide a satisfactory fit, even including quartic centrifugal distortion constants Δ_J, Δ_{JK}, and Δ_K, yielding standard deviation to experimental uncertainty ratios of $\sigma/\sigma_{exp} \approx 5.65$ and ≈3.25 (and absolute standard deviations of $\sigma \approx 0.0017$ and ≈0.0010 cm^{-1}) for $HC^{79}Br$ and $HC^{81}Br$. Indeed, as clearly evident in Fig. 2(a), the observed peak positions are visibly red-shifted with respect to the PGOPHER simulation by as much as a linewidth for higher J transition lines in the K_a: 0 ← 1 subband. We summarize these observations in more quantitative detail in Fig. S2, which displays level shifts in the $\tilde{X}(1,0,0)$ state term values (i.e., obs. – cal.) for the three observed K_a sub-manifolds (K_a = 0, 1, and 2). The clear J, K_a dependent structure (both in slope and curvature) for such an energy shift plot signals the presence of perturbations in the $\tilde{X}(1,0,0)$ manifold for both isotopologues. However, no explicit local crossing of the dark and bright state rotational ladders is observed, preventing unambiguous identification and analysis of the perturbing "dark" state. Nevertheless, the dispersed fluorescence work by Deselnicu *et al.*[27] suggests two nearby states as likely perturbers, $\tilde{X}(0,2,1)$ and $\tilde{a}(0,0,1)$, with vibrational band origins at 2897(2) and 2741(2) cm^{-1}, respectively. The $\tilde{X}(0,2,1)$ level can interact with the $\tilde{X}(1,0,0)$ level through c-type Coriolis or Fermi resonance coupling,[41] while spin–orbit interactions would mix the singlet and triplet states.[42,43] J dependent rovibrational energy level diagrams for $\tilde{X}(1,0,0)$, $\tilde{X}(0,2,1)$, and $\tilde{a}(0,0,1)$ manifolds are shown in Fig. S3, which highlights the possible suite of interacting states, with Table III summarizing our experimentally observed and theoretically predicted υ_1 CH stretch term values. Of particular note, the experimentally determined band origin from the current high resolution IR spectra (~2799.38 cm^{-1}) is in very close agreement ($\Delta\nu \approx 2$ cm^{-1}) with the assignments of Deselnicu *et al.*[27] and yet in substantial disagreement ($\Delta\nu \approx 100$ cm^{-1}) from the earlier reports of Chang *et al.*[28] By way of ancillary tests, we have carried

TABLE I. HCBr ground state spectroscopic constants (in cm^{-1}). A-reduced non-rigid Watson Hamiltonian in the I^r representation is used.

	$HC^{79}Br$				$HC^{81}Br$			
	Chang *et al.*[a]	Duan *et al.*[b]	This work[c]	This work + Duan *et al.*[d]	Chang *et al.*[a]	Duan *et al.*[b]	This work[c]	This work + Duan *et al.*[d]
A	15.534 38(17)	15.531 6(37)	15.533 65(22)	15.533 40(22)	15.534 13(16)	15.530 7(41)	15.533 42(19)	15.533 32(21)
B	0.428 838(35)	0.428 830 2(26)	0.428 830(12)	0.428 831 25(90)	0.427 246(34)	0.427 337 2(33)	0.427 320(12)	0.427 339 0(10)
C	0.416 764(35)	0.416 670 2(27)	0.416 709(11)	0.416 669 05(90)	0.415 268(34)	0.415 259 4(35)	0.415 292(11)	0.415 257 4(11)
$10^6\ \Delta_J$	0.664(34)	0.636 92(83)	0.715(96)	0.636 91(48)	0.546(31)	0.633 33(76)	0.616(93)	0.633 31(44)
$10^4\ \Delta_{JK}$	0.165(13)	0.244 77(11)	0.260(38)	0.244 792(56)	0.134(13)	0.243 315(99)	0.233(36)	0.243 346(50)
$10^2\ \Delta_K$	0.351(16)	0.08(37)	0.269 4(39)	0.264(22)	0.343(15)	−0.000 12(41)	0.270 1(35)	0.267(21)
$10^7\ \delta_J$		0.165 16(99)		0.164 97(52)		0.163 56(94)		0.163 30(50)
$10^4\ \delta_K$		0.106(13)		0.111 4(43)		0.108(17)		0.117 3(52)
$10^{12}\ \Phi_J$		−0.90(49)		−0.83(27)		−0.62(47)		−0.53(26)
$10^7\ \Phi_{KJ}$		0.124 6(44)		0.125 4(24)		0.121 9(39)		0.123 0(20)
χ_{aa}		0.011 624(53)		0.011 624(30)		0.009 726(50)		0.009 726(29)
$\chi_{bb} - \chi_{cc}$		−0.014 949(16)		−0.014 948 5(92)		−0.012 491(15)		−0.012 490 4(89)
$10^4\ C_{aa}$		1.120(46)		1.120(27)		1.236(43)		1.236(25)
$10^4\ C_{bb}$		0.026 0(22)		0.025 9(13)		0.026 1(21)		0.026 1(12)
σ/σ_{exp}[e]		3.74	1.26	2.21		3.62	1.19	2.14

[a]Chang *et al.*[63]
[b]Duan *et al.*[32] For $HC^{79}Br$, 130 hyperfine-resolved rotational lines are re-fitted using PGOPHER. For $HC^{81}Br$, 136 hyperfine-resolved rotational lines are used. Experimental uncertainty of ±0.000 001 7 cm^{-1} is assumed for all transitions.
[c]From fits to 60 and 62 ground state combination differences of $HC^{79}Br$ and $HC^{81}Br$ $\tilde{X}(1,0,0) \leftarrow \tilde{X}(0,0,0)$ transitions, respectively. Uncertainties of ±0.0003 cm^{-1} are used for both isotopologues.
[d]Uncertainties of ±0.0032 and ±0.000 001 7 cm^{-1} are used for the combination differences and microwave data, respectively.
[e]Standard deviations of the fits relative to the estimated experimental uncertainties are reported.

out high-level *ab initio* calculations coupled-cluster techniques for computational chemistry (CFOUR) at the [CCSD(T)/cc-pVQZ] level of theory,[44] which predict an anharmonic frequency of 2815.7 cm^{-1} from second-order vibrational perturbation theory (VPT2), again in more reasonable agreement ($\Delta\nu \approx 16$ cm^{-1}) with experimental observation and supporting the current assignment. Finally, the experimental C–H stretch fundamental band origin for $HC^{79}Br$ is shifted only very slightly (~0.003 cm^{-1}) to the blue with respect to $HC^{81}Br$, which is consistent with a very small fractional displacement of the Br atom in the CH stretch normal mode coordinate.

B. Hot bands $\tilde{X}(1,0,1) \leftarrow \tilde{X}(0,0,1)$ and $\tilde{X}(1,1,0) \leftarrow \tilde{X}(0,1,0)$

In addition to CH stretch fundamental $\tilde{X}(1,0,0) \leftarrow \tilde{X}(0,0,0)$ transitions, extensive progressions in two weaker additional bands are also observed in the experimental spectrum. There are no combination or overtone bands in this spectral region,[27] suggesting that they might be hot bands (i.e., of the form $v_1 + v_x \leftarrow v_x$) built on the other two vibrational modes. Indeed, by comparison of our lower state combination differences with predictions from the near-infrared work by Chang *et al.*,[32] the spectra can be unambiguously identified as CH stretch hot bands originating from $\tilde{X}(0,1,0)$ and $\tilde{X}(0,0,1)$ lower states populated in the discharge expansion. Of some dynamical interest, however, the observed intensities of $\tilde{X}(1,1,0) \leftarrow \tilde{X}(0,1,0)$ and $\tilde{X}(1,0,1) \leftarrow \tilde{X}(0,0,1)$ bands are ~0.4 and ~0.2 of the fundamental band, suggesting hot vibrational populations (unusually so for a 1D slit expansion) for the bending and C–Br stretching vibrational modes, respectively (see Sec. IV C for a more detailed discussion). Sample data high resolution Q-branches for these two hot bands are displayed in Fig. 2(b). The rotational assignments and transition frequencies for the hot bands are summarized in the supplementary material (Tables S3 and S4). Two b-type K_a subbands (K_a: 1 ← 0 and K_a: 0 ← 1) are observed for each of these hot bands. For the $\tilde{X}(1,1,0) \leftarrow \tilde{X}(0,1,0)$ transition, both K_a subbands have been successfully rotationally assigned. For the $\tilde{X}(1,0,1) \leftarrow \tilde{X}(0,0,1)$ transition, the Q-branch region of K_a: 0 ← 1 subband is highlighted in the inset, with the progression of Q-branch transitions too weak and congested to be assigned unambiguously at our current S/N [see Fig. 2(b)].

To obtain improved spectroscopic constants for the v_2 and v_3 excited states $\tilde{X}(0,0,1)$ and $\tilde{X}(0,1,0)$, we combine the current high-resolution data with previous laser spectroscopy studies on the $\tilde{A} \leftarrow \tilde{X}$ Renner–Teller electronic transition. Specifically, lower state combination differences from the $\tilde{X}(1,0,1) \leftarrow \tilde{X}(0,0,1)$ band (this work) and the $\tilde{A}(0,0,0) \leftarrow \tilde{X}(0,0,1)$ band (near-infrared work by Chang *et al.*[32]) are combined for an improved description of the v_3 mode. Similarly, for the $\tilde{X}(0,1,0)$ level, the least squares fits reported herein include lower state combination differences from the $\tilde{X}(1,1,0) \leftarrow \tilde{X}(0,1,0)$ band (this work), the $\tilde{A}(0,0,0) \leftarrow \tilde{X}(0,1,0)$ band,[32] and the $\tilde{A}(0,1,0) \leftarrow \tilde{X}(0,1,0)$ band (near-infrared work by Yu *et al.*[33]), with the upper state $\tilde{X}(1,0,1)$ and $\tilde{X}(1,1,0)$ constants determined by fixing at the improved lower state values. The best fit rotational constants for the four

TABLE II. Spectroscopic constants (in cm^{-1}) of the observed vibrationally excited states of $HC^{79}Br$ and $HC^{81}Br$.

	This work[a,b]					Chang *et al.*[c]	
	$\tilde{X}(1,1,0)$	$\tilde{X}(1,0,1)$[d]	$\tilde{X}(1,0,0)$	$\tilde{X}(0,1,0)$[e]	$\tilde{X}(0,0,1)$[e]	$\tilde{X}(0,1,0)$	$\tilde{X}(0,0,1)$
				$HC^{79}Br$			
Origin	3916.163 0(10)	3477.359 85(31)	2799.38 442(49)	1117.70	676.443 6	1117.70(2)	676.443 6(25)
A	13.297 0(12)	14.896 9	14.993 51(52)	16.106 6(60)	15.518 5	16.098 33(36)	15.518 5(29)
B	0.425 545(24)	0.424 773(21)	0.428 625(15)	0.428 377(40)	0.425 322(28)	0.428 347(31)	0.425 297(25)
C	0.415 469(30)	0.411 694(10)	0.415 961(13)	0.415 238(41)	0.413 271(30)	0.415 191(31)	0.413 225(25)
$10^6\ \Delta_J$	−1.56(14)	0.636 91	0.586(71)	0.447(53)	0.78(12)	0.581(27)	0.489(56)
$10^4\ \Delta_{JK}$	25.35(22)	0.244 792	0.418(25)	0.422(94)	0.244 792	0.165	0.165
$10^2\ \Delta_K$	0.264	0.264	2.121(12)	0.32(13)	0.264	0.351	0.351
σ/σ_{exp}[f]	4.55	0.99	5.65	2.35	0.94	1.24	1.36
				$HC^{81}Br$			
Origin	3916.057 04(83)	3476.081 99(11)	2799.381 59(29)	1117.63	675.276 1	1117.63(2)	675.276 1(28)
A	13.304 30(100)	14.896 5	14.990 36(32)	16.108 4(44)	15.524 2	16.096 56(36)	15.524 2(33)
B	0.424 137(21)	0.423 308 5(28)	0.427 105(10)	0.426 914(26)	0.423 839(50)	0.426 827(32)	0.423 803(19)
C	0.414 044(27)	0.410 380 6(34)	0.414 503 8(83)	0.413 884(27)	0.411 871(47)	0.413 739(32)	0.411 853(19)
$10^6\ \Delta_J$	−1.53(12)	0.633 31	0.622(47)	0.627(36)	0.81(15)	0.517(28)	0.576(31)
$10^4\ \Delta_{JK}$	25.12(19)	0.243 346	0.272(16)	0.319(88)	0.243 346	0.134	0.134
$10^2\ \Delta_K$	0.267	0.267	2.219 2(73)	0.483(82)	0.267	0.343	0.343
σ/σ_{exp}[f]	3.74	0.36	3.25	1.50	1.76	1.34	1.38

[a]Experimental uncertainties of 0.0003 cm^{-1} are assumed for the fundamental band of the two isotopologues. For the two hot bands, uncertainties of 0.0010 and 0.0020 cm^{-1} are used for the stronger and weaker lines, respectively.
[b]For quartic centrifugal distortion constants if the values are reported without uncertainties, they are fixed at ground state values.
[c]Chang *et al.*[32]
[d]Only the K_a: 1 ← 0 subband is assigned for the $\tilde{X}(1,0,1) \leftarrow \tilde{X}(0,0,1)$ transition. Therefore, to estimate the band origin of the upper state, a rotational constant (A) is computed from its ground state value and the experimentally derived vibration–rotation interaction constants. The estimated uncertainties of the A constants are 0.0033 and 0.0036 cm^{-1} for $HC^{79}Br$ and $HC^{81}Br$.
[e]Only energy differences between the two vibrationally excited states can be obtained from the hot bands. Therefore, the band origins of $\tilde{X}(0,1,0)$ and $\tilde{X}(0,0,1)$ in the fits are fixed at values previously determined at higher precision in Ref. 32.
[f]Standard deviation of the fits relative to the estimated experimental uncertainties.

TABLE III. Observed and calculated vibrational term energies (in cm^{-1}) of the HCBr fundamental and combination bands.

	Experimental			CCSD(T)[a]	
	This work[b]	Deselnicu *et al.*[c]	Chang *et al.*[d]	Harmonic	Anharmonic[e]
$\tilde{X}(1,0,0)$	2799.384 42(49) 2799.381 59(29)	2802(2)	2901(4)	2951.0	2815.7
$\tilde{X}(1,0,1)$	3477.359 9(33) 3476.082 0(36)	3479(2)	⋯	3651.9	3506.7
$\tilde{X}(1,1,0)$	3916.163 0(10) 3916.057 04(83)	3917(2)	⋯	4111.4	3941.6

[a]Coupled cluster [CCSD(T)] calculation with a cc-pVQZ basis set.
[b]Top and bottom values are for $HC^{79}Br$ and $HC^{81}Br$, respectively. Experimental uncertainties are in parentheses.
[c]Deselnicu *et al.*[27]
[d]Chang *et al.*[28]
[e]Second-order vibration perturbation theory (VPT2) using the frozen-core ANO2 basis set is used to calculate the anharmonic frequency.

TABLE IV. Summary of vibration–rotation interaction constants α_i^X for the singlet ground state $\tilde{X}^1A'$ of $HC^{79}Br$ and $HC^{81}Br$.[a,b]

	$HC^{79}Br$			$HC^{81}Br$		
	α_i^A	α_i^B	α_i^C	α_i^A	α_i^B	α_i^C
ν_1 CH str.	0.622(2) [0.5842]	0.000 1(1) [0.0004]	0.000 7(1) [0.0007]	0.543(2)	0.0001(1)	0.000 7(2)
ν_2 bend	−0.573(6) [−0.4623]	0.000 45(5) [0.0005]	0.001 43(4) [0.0015]	−0.55(2)	0.0006(6)	0.001 3(6)
ν_3 CBr str.	0.0149(29) [0.0222]	0.003 50(3) [0.0033]	0.003 40(3) [0.0033]	0.0091(33)	0.0035(1)	0.003 40(5)

[a] *Ab initio* predicted vibration–rotation constants from coupled cluster [CCSD(T)] calculation with an cc-pVQZ basis set are given in square brackets.
[b] Experimental uncertainties are in parentheses.

vibrationally excited states of $HC^{79}Br$ and $HC^{81}Br$ are reported in Table II, with Table III summarizing vibrational term values from high resolution IR analysis of the fundamental and hot band data. Agreement between the observed vibrational term values and predictions from previous emission spectroscopic studies is excellent (i.e., within 1 σ uncertainty).

Taking this analysis a step further, the experimentally determined rotational constants of the vibrationally excited states $\tilde{X}(0,0,1)$, $\tilde{X}(0,1,0)$, and $\tilde{X}(1,0,0)$ allow us to estimate the vibration–rotation constants α_i^X using

$$X_v = X_0 - \sum_i \alpha_i^X v_i, \tag{2}$$

where X_v is the vibrationally dependent rotational constant ($X = A, B, or\ C$), X_0 represents the ground state rotational constant, and v_i is the vibrational quantum number. Table IV represents a summary comparison between experimental and *ab initio* predicted vibration–rotation constants, indicating good qualitative agreement (i.e., in both sign and magnitude). Most notably, the CH stretching vibration results in a significant decrease (−4.0%) in the A rotational constant, with a comparable increase (+3.7%) in A upon excitation of the HCBr bending vibration, due to an increase in the vibrationally averaged C–H bond length and H–C–Br bond angle upon excitation in ν_1 and ν_2, respectively. The B and C rotational constants are much less sensitive to such vibrational averaging but, as expected, are clearly more affected by excitation of the ν_3 C–Br stretch vibration.

IV. DISCUSSION

A. Partially resolved hyperfine structure due to Br atom nuclear spin effects

Due to collisional collimation and therefore spontaneous narrowing of transverse velocities in the slit-jet supersonic expansion geometry, the infrared resolution achieved is intrinsically reduced-Doppler. For a Ne/He expansion, this translates into instrumental Gaussian linewidth (full width at half maximum) ≈ 60 MHz, which proves sufficient to permit for observation of a nuclear spin hyperfine structure due to the Br atom, even in the infrared. This structure arises from coupling between the nuclear spin angular momentum **I** and rotational angular momentum **J** to form **F** = **J** + **I**. Both ^{79}Br and ^{81}Br isotopes have a nuclear spin of I = 3/2, with previous microwave studies[31] having accurately determined the HCBr nuclear quadrupole and nuclear spin-rotation coupling constants for the ground vibrational state. By way of example, Fig. 3 (left panel) shows a high resolution blow up spectral region for the b-type K_a: 2 ← 1 Q-branches, highlighting the broadening (and indeed even partial splitting) of the low J rovibrational lines due to a nuclear spin hyperfine structure. In the interest of simplicity, the simulated stick diagrams assume identical hyperfine constants for both ground and upper states at a rotational temperature of 35 K. Convolution of these stick diagrams over an instrumental Gaussian line shape ($\Delta\nu$ = 60 MHz) predicts a detailed spectral scan (green) in remarkably quantitative agreement with the experiment.

For these lowest J levels, these nuclear spin splittings become even more pronounced, as the magnitudes of the spin (**I**) and rotational angular momenta (**J**) become comparable, thereby making a hyperfine structure in the transition lines more easily resolvable. By way of example, Fig. 3 (right panel) features the isolated 4_{22} ← 4_{13} rovibrational Q branch line of $HC^{81}Br$, with the corresponding hyperfine energy levels for the labeled transitions shown. At this low J, the hyperfine contribution to this rovibrational line is partially resolved into a clear doublet structure, with the ~0.0027 cm^{-1} separation between two peaks in excellent agreement with ground state predictions. Unfortunately, the structures in these hyperfine broadened and split transitions are not sufficient to warrant extracting independent nuclear hyperfine constants for the vibrationally excited state. However, it is fair to say that even this level of resolution of hyperfine structure would not be possible with conventional Doppler broadened spectroscopy in the mid-infrared (3–5 μm).

B. Boltzmann intensity analysis of the $\tilde{X}(1,0,0) \leftarrow \tilde{X}(0,0,0)$ band reveals "charge-sloshing" rotation in the vibrational transition dipole moment direction

To more quantitatively explore the nature of a- and b-type bands in the $\tilde{X}(1,0,0) \leftarrow \tilde{X}(0,0,0)$ transition and understand the

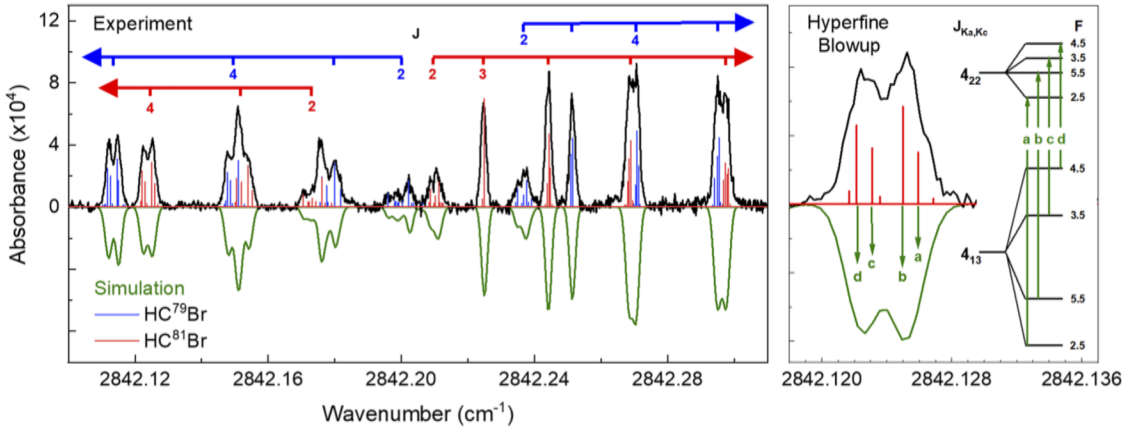

FIG. 3. Left panel: Details of the partially resolved hyperfine structure in the Q-branches of the $HC^{79}Br$ and $HC^{81}Br$ $\tilde{X}(1,0,0) \leftarrow \tilde{X}(0,0,0)$ K_a: 2 ← 1 subbands. The PGOPHER simulated spectrum (green and inverted) assumes a rotational temperature of 35 K and instrumental linewidths of 60 MHz. The red and blue stick spectra are the predicted transition frequencies for $HC^{79}Br$ and $HC^{81}Br$ using nuclear quadrupole and nuclear spin-rotation coupling constants from the kinetic microwave study.[31] Right panel: $HC^{81}Br$ $4_{22} \leftarrow 4_{13}$ rovibrational feature. a–d denote transitions between hyperfine levels arising from the coupling between rotational and nuclear spin angular momentum, with total angular momentum $\mathbf{F} = \mathbf{J} + \mathbf{I}$.

direction of transition dipole moment during C–H stretching, we perform a Boltzmann analysis of the rovibrational transition intensities. For a near prolate asymmetric top, the line strength (S) of a rovibrational absorption transition under thermal equilibrium conditions is well approximated by[45]

$$S = S_0 A\left(J'', K''\right)\left(2J''+1\right) e^{-\frac{\tilde{E}\left(J'', K_a'', K_c''\right)}{kT_{rot}}}, \tag{3}$$

where S_0 is proportional to the total line strength for a given a-, b-, or c-type band, $A\left(J'', K''\right)$ is the prolate symmetric top Hönl–London factor[45] (within 2% of the exact asymmetric top line strengths and >5× more accurate than our 10% intensity uncertainties), $\left(2J''+1\right)$ is the degeneracy of the lower state, $\tilde{E}\left(J'', K_a'', K_c''\right)$ is the rotational energy with respect to the ground state, and T_{rot} is the rotational temperature. The Boltzmann analysis predicts a linear relationship between $\ln\left[S/A\left(J'', K''\right)\left(2J''+1\right)\right]$ $\{$i.e., $ln\left[Pop/\left(2J''+1\right)\right]\}$ and rotational energy, with a slope of $-1/kT_{rot}$ and the y-intercepts indicating relative integrated line strengths of the three observed bands. Furthermore, since the two Br isotopologues are present in nearly identical abundance, the $HC^{79}Br$ and $HC^{81}Br$ results can be "co-added" and thus signal averaged into a single linear fit. Moreover, since both a- and b-type transitions arise from an identical lower state, the two sets of data points carry the same information and should be well described by a common rotational temperature. The resulting Boltzmann plots for a/b type and $^{79}Br/^{81}Br$ species are presented in Fig. 4, which reveal rotationally cold HCBr radicals at a global rotational temperature of 34.5 ± 0.6 K. We furthermore found that the radical rotational temperatures increase with the applied electric field and thus current in the discharge region. As this magnitude of the applied electric field increases from 5.2 to 8.4 kV/cm (and the corresponding discharge current increases from 77 to 250 mA), the rotational temperature of the jet-cooled radicals grows smoothly from 24 to 35 K.

From quantitative least squares fits to the y-intercepts, the relative b- to -a-type transition line strength is found to be 3.00(8), which for a predicted line strength ratio of $I_A/I_B = \tan^2(\phi_{exp})$ corresponds to an angle of $\phi_{exp} \approx 30.0(4)°$ between the transition dipole moment $(\partial\boldsymbol{\mu}/\partial Q)_{exp}$ and the B principal rotation axis. To put that in context, CCSD(T)/cc-pVQZ *ab initio* calculations for the optimized geometry predict a H–C–Br bond angle of 101.2°, with a clockwise

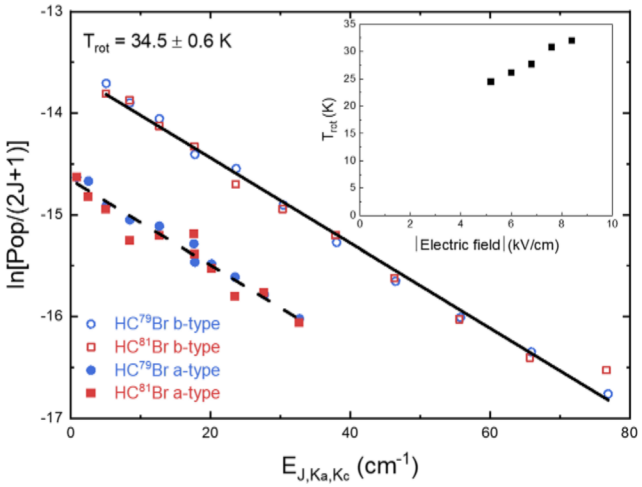

FIG. 4. Boltzmann plot for the b-type (empty data points) and a-type transitions (solid data points) of the $HC^{79}Br$ (blue circles) and $HC^{81}Br$ (red squares) $\tilde{X}(1,0,0) \leftarrow \tilde{X}(0,0,0)$ band. The black solid and dashed lines are the linear least-squares fits to the b-type and a-type transitions, showing a common rotational temperature of 34.5 ± 0.6 K. The y-intercepts of the b-type and a-type transitions are −13.60 ± 0.02 and −14.65 ± 0.02, respectively, corresponding to a ratio of b-type to a-type line strength of 3.00(8). Inset: Dependence of jet-cooled HCBr rotational temperature on the applied electric field in the discharge system.

2.9° tilt of the C–Br bond away from the A inertial axis (see Fig. 1). From a simple bond-dipole model (where the vibrational transition moment arises through normal mode displacement of static charges fixed on the various atoms), the predicted $(\partial\boldsymbol{\mu}/\partial Q)_{\text{bond-dipole}}$ deviates substantially from the experimentally determined transition moment $(\partial\boldsymbol{\mu}/\partial Q)_{\text{exp}}$, with clockwise rotation of 15.9(4)° between the two vectors (see Fig. 1). The failure of this simple picture in accurately predicting the transition dipole moment direction arises from neglecting changes in the dipolar charge distribution q_i while stretching the C–H bond, which can contribute to the transition dipole moment by the additional chain rule term,

$$\frac{\partial \boldsymbol{\mu}}{\partial Q} = \sum_i q_i \left(\frac{\partial \boldsymbol{r_i}}{\partial Q}\right) + \sum_i \boldsymbol{r_i}\left(\frac{\partial q_i}{\partial Q}\right). \tag{4}$$

Such vibrationally induced "charge sloshing" effects were identified by Whitney *et al.* in high resolution infrared studies of the CH_2Cl radical[46] and have been subsequently predicted and observed in many radical and molecular ion spectroscopic studies.[47–52] This increase in angle ϕ_{exp} between $(\partial\boldsymbol{\mu}/\partial Q)_{\text{exp}}$ and the B axis is attributed to additional electron flow along the highly dipolar C–Br bond from stretching of the C–H bond. By way of further *ab initio* support, electron densities have been calculated [DFT/B3LYP/6-311++g(3df,3pd)] at the equilibrium geometry and for small (±0.1 Å) displacements along the normal mode C–H bond coordinate, from which theoretical differential charge isocontours due to CH bond stretching can be obtained. The results are plotted in Fig. 5, which reveals significant CH vibrationally induced flow of electron density from the C to Br atom. This "charge-sloshing" dynamics lead to clockwise rotation of $(\partial\boldsymbol{\mu}/\partial Q)_{\text{exp}}$ away from the B axis and thus enhancement of a-type vs b-type transitions in the rovibrational spectra.

C. Vibrational excitation and relaxation in a supersonic slit-jet discharge

In addition to fundamental transitions from the ground state $\tilde{X}(0,0,0)$, the experimental spectra reveal rovibrational transitions arising from two vibrationally excited states, $\tilde{X}(0,0,1)$ and $\tilde{X}(0,1,0)$, at 676 and 1118 cm^{-1} higher energies. This is at first surprising as the much higher densities in a slit jet vs pinhole expansion are known to promote significant cooling of low frequency vibrational states.[53–55] In order to explore the reasons for such non-equilibrium vibrational dynamics in HCBr radicals, we first make the reasonable assumption of zero change in the Δv = +1 fundamental vs hot band oscillator strengths. In this approximation, the HCBr vibrational densities with respect to the ground state $\tilde{X}(0,0,0)$ can be readily determined from the Boltzmann analysis intercepts of all three bands under a common rotational temperature (see Fig. S4), with the relative populations in the $\tilde{X}(0,0,0)$, $\tilde{X}(0,0,1)$, and $\tilde{X}(0,1,0)$ manifolds visually summarized in Fig. 6. With only single quanta excitation in the bending and C–Br stretching vibration observed, a crude estimate of vibrational temperature for each of the two modes can be made from a Boltzmann distribution,

$$\ln\left[\frac{S(v_i)}{S_0}\right] = -\frac{1}{kT_{vib}}\tilde{G}(v_i), \tag{5}$$

where $S(v_i)$ and S_0 are integrated intensities of rovibrational bands from the $v_i = 1$ vibrational state and ground vibrational state, respectively, $\tilde{G}(v_i)$ is the term energy of the $v_i = 1$ state, and T_{vib} is the vibrational temperature. For HCBr bending (v_2) and C–Br stretching (v_3) degrees of freedom, we estimate $T_{\text{vib}} \approx 1771$ and 643 K, i.e., revealing both a hot and clearly non-equilibrium distribution among the different vibrational modes.

Vibrational excitation in molecular beam discharge sources has been observed previously in many polyatomic molecules.[56–58] In particular, Sanz *et al.*[59] systematically studied vibrational excitation and relaxation of five linear polyatomic molecules, OCS, OC_3S, HC_3N, HC_5N, and SiC_2S in a DC discharge followed by a pinhole axisymmetric supersonic expansion. Vibrational excitations are

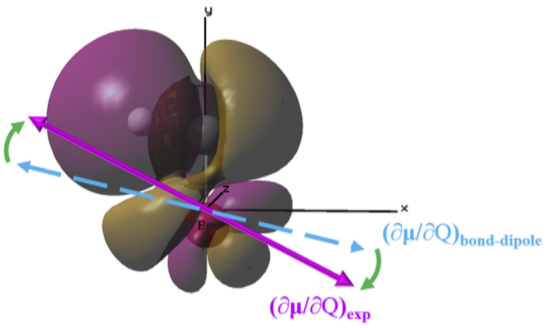

FIG. 5. *Ab initio* HCBr wavefunction differential charge density (0.0001 isovalue) computed by subtracting the wavefunction electron density at +0.1 Å displacement along the C–H stretch normal mode coordinate from the electron density at equilibrium geometry. The increase and decrease of electron densities are shown in gold and purple, respectively, calculated at the B3LYP/6-311++g(3df,3pd) level of theory. Note the clockwise rotation by 15.9(4)° of the transition dipole moment *away from* the C–H bond-dipole direction due to synchronous CH stretch induced charge flow along the C–Br bond (i.e., "charge-sloshing").

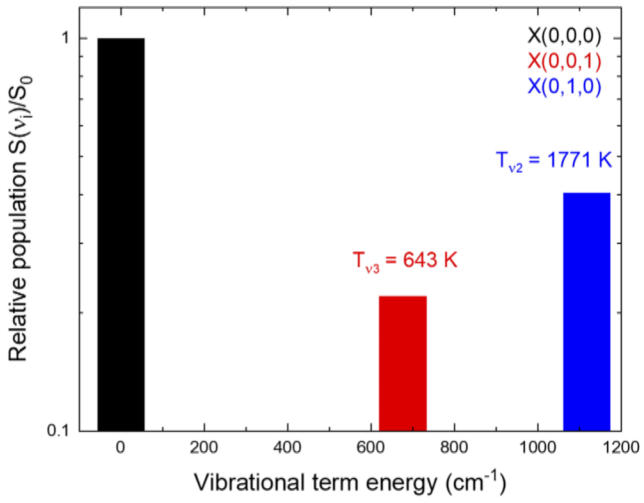

FIG. 6. Relative population of the $\tilde{X}(0,0,0)$, $\tilde{X}(0,0,1)$, and $\tilde{X}(0,1,0)$ levels (normalized to population in the ground vibrational level). Approximated from a simple two state Boltzmann distribution, vibrational temperatures of 643 and 1771 K are found for the C–Br stretching and bending vibrational modes.

attributed to inelastic vibrational energy transfer with energetic electrons and excited metastable rare gas atoms in the plasma. During the subsequent supersonic expansion, however, vibration relaxation can occur via two pathways, vibration–vibration (VV) and vibration–translation (VT) energy transfer.[60–62] Intra- and intermolecular VV energy transfer in polyatomics can be accelerated by small energy gaps and typically occurs very fast, resulting in rapid equilibration within a vibrational manifold. Particularly for comparable energy vibrations, both intra- and inter-molecular VV energy transfer are facile and lead to rapid equilibration between vibrational modes.[60,62] By way of contrast, VT energy transfer typically is extremely inefficient for vibrational spacings significantly higher than collisional energies (kT_{trans}) present in the discharge and/or expansion region[59] (cf. kT ≈ 207 cm^{-1} at 298 K). Such mechanisms for vibrational excitation and relaxation are consistent with our observations: (i) The applied electric field in the discharge region is −8.4 kV/cm (~250 mA discharge current), which for an approximate mean free path of $\lambda \approx 10\ \mu m$ at 390 mbar generates electron temperatures easily sufficient to excite HCBr bend and CBr stretch modes prior to the slit expansion exit orifice. (ii) Excitation in both HCBr bend and CBr stretch degrees of freedom has energies $\tilde{G}(v_i) > kT$, which, due to the slow VT energy transfer, are only inefficiently cooled on the few tens of μs timescale of the supersonic expansion. (iii) The two vibrational modes observed are not in collisional equilibrium, arising from inefficient non-resonant VV energy transfer and presumably due to large differences in vibrational frequencies (677 and 1119 cm^{-1} for C–Br stretching and bending modes, respectively).[59]

In addition to VT energy transfer via inelastic collisions with energetic plasma electrons, a non-equilibrium distribution of vibrational energy can be explained in a Franck–Condon description[58] by changes in H–C–Br bond angle/C–Br bond length in the dissociative electron attachment process (i.e., $HCBr_3 \rightarrow HCBr_2 \rightarrow HCBr \rightarrow HC$). In support of this argument, equilibrium geometries of the precursor $HCBr_3$ and intermediate $HCBr_2$ and HCBr species have been calculated using high level CCSD(T) methods in a cc-PVQZ basis set, which reveal a significant decrease in HCBr angle (θ_{HCBr} = 101.2°) compared with $HCBr_2$ (θ_{HCBr2} = 117.5°). Indeed, one anticipates such behavior from simple freshman chemistry ideas, as the lone electron pairs on the C atom take up more space than filled molecular bonding orbitals and make the molecule more bent. Interestingly, smaller effects are evident in the C–Br bond lengths, specifically 1.850 and 1.849 Å for $HCBr_2$ and HCBr, respectively. Based on a sudden Franck–Condon picture for electron dissociative attachment, the more significant change in H–C–Br bond angle vs C–Br bond length therefore helps rationalize "hotter" excitation in the ν_2 bend vs the ν_3 C–Br stretch modes.

V. CONCLUSION

We report the first high-resolution, reduced-Doppler spectrum of the jet-cooled singlet bromomethylene HCBr in the C–H stretching (υ_1) region around 2800 cm^{-1}. Both the CH stretch fundamental and two additional vibrational hot bands (HCBr bend and CBr stretch) are fully rotationally resolved and assigned, specifically $\tilde{X}(1,0,0) \leftarrow \tilde{X}(0,0,0)$, $\tilde{X}(1,1,0) \leftarrow \tilde{X}(0,1,0)$, and $\tilde{X}(1,0,1) \leftarrow \tilde{X}(0,0,1)$. High resolution rotational analysis of the observed transitions is performed, with precision rotational constants for the upper $\tilde{X}(1,0,0)$, $\tilde{X}(1,0,1)$, and $\tilde{X}(1,1,0)$ states reported for the first time and vibration–rotation interaction constants for the three vibrational modes of HCBr obtained and compared to high level CCSD(T)/cc-PVQZ calculations. The experimentally determined term value for the fundamental band $\tilde{X}(1,0,0)$ is found to be 2799.38 cm^{-1}, with combination band term values at ~3477 and ~3916 cm^{-1} for $\tilde{X}(1,0,1)$ and $\tilde{X}(1,1,0)$, respectively. The results are all in excellent agreement ($\Delta\nu \approx +/-2\ cm^{-1}$) with previous fluorescence emission spectroscopic studies[27,28] and unambiguously resolve disagreements in the literature about the ν_1 CH stretch band origin for HCBr.

For the fundamental band, a standard non-rigid Watson asymmetric top Hamiltonian yields least squares fits well outside of our experimental uncertainty, signaling the presence of weak perturbations in the upper state $\tilde{X}(1,0,0)$ level. Two possible sources of perturbation are identified as the c-type Coriolis coupling with the $\tilde{X}(0,2,1)$ state and the spin–orbit interaction with the triplet $\tilde{a}(0,0,1)$ state. However, no local rotational crossings are observed in the jet-cooled spectrum necessary to rigorously identify the perturbing state vibrational band origin and rotational constants. It is worth noting, however, that room temperature studies provide spectral access to considerably higher J and K_a levels where such crossings might be observed and thereby potentially provide additional detailed information on the perturbing manifold. As a result of reduced-Doppler resolution (~60 MHz) in the slit jet expansion, the ^{79,81}Br nuclear spin hyperfine structure (e.g., broadening and splitting) is observed in the infrared. The measured ratio of a-type to b-type band intensities permits for experimental specification of the transition dipole moment vector, rotated significantly from that of simple bond-dipole model predictions and arising from CH stretch vibrationally induced "charge-sloshing" dynamics along the polar C–Br bond.

Finally, we see significant populations of HCBr in the ν_2 = 1 H–C–Br bend and ν_3 = 1 C–Br stretch vibrational state, which is surprising for the high collision number and slow density drop off in a slit supersonic expansion. We attribute such vibrational populations to either (i) inelastic collisions with energetic electrons produced in the discharge[59] or (ii) the Franck–Condon-like excitation during the radical generation process due to changes in HCBr bond angle and/or CBr length.[58] Regardless of origin, vibrational excitation in HCBr is clearly poorly cooled during the supersonic expansion due to extremely inefficient VT energy transfer,[58] with rough vibrational temperature estimates of 1771 and 643 K for the bending and C–Br stretching modes.

SUPPLEMENTARY MATERIAL

See the supplementary material for analysis of dark state perturbations, additional spectral bands, tabulated spectral transitions, and modeling of HCBr formation kinetics in the slit discharge source.

ACKNOWLEDGMENTS

This work was supported by grants from the Department of Energy (Grant No. DE-FG02-09ER16021), with initial funds for construction of the slit-jet laser spectrometer provided by the National Science Foundation (Grant Nos. CHE 1665271/2053117

and PHY 1734006). We thank Professor Scott Reid for discussions and sharing unpublished results from the Reid group's laser induced fluorescence studies and Professor John Stanton for his ever patient and helpful guidance with CFOUR *ab initio* calculations.

AUTHOR DECLARATIONS

Conflict of Interest

The authors have no conflicts to disclose.

DATA AVAILABILITY

The data that support the findings of this study are available within the article and its supplementary material.

REFERENCES

[1]R. A. Moss, M. Platz, and M. Jones, Jr., *Reactive Intermediate Chemistry* (Wiley-Interscience, Hoboken, NJ, 2004).
[2]W. Kirmse, *Carbene Chemistry* (Elsevier, 2013).
[3]R. A. Moss and M. P. Doyle, *Contemporary Carbene Chemistry* (Wiley, Hoboken, 2013).
[4]W. v. E. Doering, R. G. Buttery, R. G. Laughlin, and N. Chaudhuri, "Indiscriminate reaction of methylene with the carbon-hydrogen bond," J. Am. Chem. Soc. **78**, 3224 (1956).
[5]D. B. Richardson, M. C. Simmons, and I. Dvoretzky, "The reactivity of methylene from photolysis of diazomethane," J. Am. Chem. Soc. **82**, 5001–5002 (1960).
[6]H. M. L. Davies, T. Hansen, and M. R. Churchill, "Catalytic asymmetric C–H activation of alkanes and tetrahydrofuran," J. Am. Chem. Soc. **122**, 3063–3070 (2000).
[7]M.-D. Su, "Role of spin–orbit coupling and symmetry in triplet carbenic addition chemistry," J. Phys. Chem. **100**, 4339–4349 (1996).
[8]A. Fürstner, C. Nevado, M. Waser, M. Tremblay, C. Chevrier, F. Teplý, C. Aïssa, E. Moulin, and O. Müller, "Total synthesis of iejimalide A–D and assessment of the remarkable actin-depolymerizing capacity of these polyene macrolides," J. Am. Chem. Soc. **129**, 9150–9161 (2007).
[9]J. A. McCauley, M. T. Rudd, K. T. Nguyen, C. J. McIntyre, J. J. Romano, K. J. Bush, S. L. Varga, C. W. Ross III, S. S. Carroll, J. DiMuzio, M. W. Stahlhut, D. B. Olsen, T. A. Lyle, J. P. Vacca, and N. J. Liverton, "Bismacrocyclic inhibitors of hepatitis C NS3/4a protease," Angew. Chem., Int. Ed. **47**, 9104–9107 (2008).
[10]K. B. Eisenthal, R. A. Moss, and N. J. Turro, "Divalent carbon intermediates: Laser photolysis and spectroscopy," Science **225**, 1439–1445 (1984).
[11]H. F. Schaefer, "Methylene: A paradigm for computational quantum chemistry," Science **231**, 1100–1107 (1986).
[12]J. M. Foster and S. F. Boys, "Quantum variational calculations for a range of CH_2 configurations," Rev. Mod. Phys. **32**, 305 (1960).
[13]L. B. Harding and W. A. Goddard III, "Methylene: *Ab initio* vibronic analysis and reinterpretation of the spectroscopic and negative ion photoelectron experiments," Chem. Phys. Lett. **55**, 217–220 (1978).
[14]D. G. Leopold, K. K. Murray, A. E. S. Miller, and W. C. Lineberger, "Methylene: A study of the $\tilde{X}\,^3B_1$ and $\tilde{a}\,^1A_1$ states by photoelectron spectroscopy of CH_2^- and CD_2^-," J. Chem. Phys. **83**, 4849–4865 (1985).
[15]S. H. Kable, S. A. Reid, and T. J. Sears, "The halocarbenes: Model systems for understanding the spectroscopy, dynamics and chemistry of carbenes," Int. Rev. Phys. Chem. **28**, 435–480 (2009).
[16]R. Renner, "Zur theorie der wechselwirkung zwischen elektronen-und kernbewegung bei dreiatomigen, stabförmigen molekülen," Z. Phys. **92**, 172–193 (1934).
[17]H. Fan, I. Ionescu, C. Annesley, and S. A. Reid, "Lifetime lengthening and the Renner–Teller effect in the HCF ($\tilde{A}^1A'' \leftarrow \tilde{X}^1A'$) system," Chem. Phys. Lett. **378**, 548–552 (2003).
[18]T. W. Schmidt, G. B. Bacskay, and S. H. Kable, "Ab initio potential energy surface and vibrational frequencies of $\tilde{A}(^1A'')$ HCF," Chem. Phys. Lett. **292**, 80–86 (1998).
[19]B. C. Chang and T. J. Sears, "Rotationally resolved near-infrared spectrum of the HCCI $\tilde{A}^1A'' \leftarrow \tilde{X}^1A'$ transition," J. Mol. Spectrosc. **173**, 391–403 (1995).
[20]B. C. Chang and T. J. Sears, "High resolution near infrared electronic spectroscopy of HCBr," J. Chem. Phys. **105**, 2135–2140 (1996).
[21]C. Tao, C. Ebben, H.-T. Ko, and S. A. Reid, "First observation of the elusive iodocarbene: Ground state multiplicity and singlet–triplet gap of CHI," Phys. Chem. Chem. Phys. **10**, 6090–6092 (2008).
[22]C. G. Stevens and J. C. D. Brand, "Angular momentum dependence of first- and second-order singlet-triplet interactions in polyatomic molecules," J. Chem. Phys. **58**, 3324–3330 (1973).
[23]R. J. Butcher, S. Saito, and E. Hirota, "Magnetic properties of the $\tilde{A}^1A''$ state of HCF," J. Chem. Phys. **80**, 4000–4002 (1984).
[24]M. K. Gilles, K. M. Ervin, J. Ho, and W. C. Lineberger, "Negative ion photoelectron spectroscopy of halocarbene anions (HCF–, $HCCl^-$, $HCBr^-$, and HCI^-); photoelectron angular distributions and neutral triplet excitation energies," J. Phys. Chem. **96**, 1130–1141 (1992).
[25]C. Tao, C. Mukarakate, and S. A. Reid, "Fluorescence excitation and single vibronic level emission spectroscopy of the $\tilde{A}^1A'' \leftarrow \tilde{X}^1A'$ system of CHCl," J. Chem. Phys. **124**, 224314 (2006).
[26]C.-S. Lin, Y.-E. Chen, and B.-C. Chang, "New electronic spectra of the HCCl and DCCl $\tilde{A}$–$\tilde{X}$ vibronic bands," J. Chem. Phys. **121**, 4164–4170 (2004).
[27]M. Deselnicu, C. Tao, C. Mukarakate, and S. A. Reid, "Fluorescence excitation and emission spectroscopy of the $\tilde{A}^1A'' \leftarrow \tilde{X}^1A'$ system of CHBr," J. Chem. Phys. **124**(13), 134302 (2006).
[28]W.-Z. Chang, H.-J. Hsu, and B.-C. Chang, "New dispersed fluorescence spectra of HCBr and DCBr," Chem. Phys. Lett. **413**, 25–30 (2005).
[29]T.-C. Tsai, C.-W. Chen, and B.-C. Chang, "Laser excitation and dispersed fluorescence spectra of the HCBr $\tilde{A}$–$\tilde{X}$ vibronic transition," J. Chem. Phys. **115**, 766–770 (2001).
[30]C. Tao, C. Mukarakate, Z. Terranova, C. Ebben, R. H. Judge, and S. A. Reid, "High resolution study of spin-orbit mixing and the singlet-triplet gap in chlorocarbene: Stimulated emission pumping spectroscopy of $CH^{35}Cl$ and $CD^{35}Cl$," J. Chem. Phys. **129**, 104309 (2008).
[31]C. Duan, M. Hassouna, A. Walters, M. Godon, P. Dréan, and M. Bogey, "Rotational spectrum of HCBr produced by 193-nm laser photolysis of bromoform," J. Mol. Spectrosc. **220**(1), 113–121 (2003).
[32]B.-C. Chang, J. Guss, and T. J. Sears, "Hot bands in the spectrum of HCBr," J. Mol. Spectrosc. **219**, 136–144 (2003).
[33]H.-G. Yu, T. Gonzalez-Lezana, A. J. Marr, J. T. Muckerman, and T. J. Sears, "Experimental and theoretical studies of the near-infrared spectrum of bromomethylene," J. Chem. Phys. **115**, 5433–5444 (2001).
[34]S. Davis, M. Fárník, D. Uy, and D. J. Nesbitt, "Concentration modulation spectroscopy with a pulsed slit supersonic discharge expansion source," Chem. Phys. Lett. **344**, 23–30 (2001).
[35]P. Zou, J. Shu, T. J. Sears, G. E. Hall, and S. W. North, "Photodissociation of bromoform at 248 nm: Single and multiphoton processes," J. Phys. Chem. A **108**, 1482–1488 (2004).
[36]C. Blondel, P. Cacciani, C. Delsart, and R. Trainham, "High-resolution determination of the electron affinity of fluorine and bromine using crossed ion and laser beams," Phys. Rev. A **40**, 3698–3701 (1989).
[37]E. Riedle, S. H. Ashworth, J. T. Farrell, and D. J. Nesbitt, "Stabilization and precise calibration of a continuous wave difference frequency spectrometer by use of a simple transfer cavity," Rev. Sci. Instrum. **65**, 42–48 (1994).
[38]A. S. Pine, "High-resolution methane ν_3 band spectra using a stabilized tunable difference-frequency laser system," J. Opt. Soc. Am. **66**, 97–108 (1976).
[39]C. M. Western, "PGOPHER: A program for simulating rotational, vibrational and electronic spectra," J. Quant. Spectrosc. Radiat. Transfer **186**, 221–242 (2017).
[40]J. K. Watson, *Vibrational Spectra and Structure* (Elsevier, Amsterdam, 1977).
[41]K. D. Doney, A. Kortyna, and D. J. Nesbitt, "High-resolution infrared spectroscopy of HCF in the CH stretch region," J. Chem. Phys. **152**, 014305 (2020).
[42]S. Nyambo, C. Karshenas, S. A. Reid, P. Lolur, and R. Dawes, "Towards a global model of spin-orbit coupling in the halocarbenes," J. Chem. Phys. **142**, 214304 (2015).

[43]H. Petek, D. J. Nesbitt, C. B. Moore, F. W. Birss, and D. A. Ramsay, "Visible absorption and magnetic rotation spectroscopy of $^1CH_2$: Analysis of the $^1A_1$ state and the $^1A_1$–$^3B_1$ coupling," J. Chem. Phys. **86**, 1189–1205 (1987).
[44]D. A. Matthews, L. Cheng, M. E. Harding, F. Lipparini, S. Stopkowicz, T.-C. Jagau, P. G. Szalay, J. Gauss, and J. F. Stanton, "Coupled-cluster techniques for computational chemistry: The CFOUR program package," J. Chem. Phys. **152**, 214108 (2020).
[45]G. Herzberg, *Molecular Spectra and Molecular Structure. Vol. 2: Infrared and Raman Spectra of Polyatomic Molecules* (Van Nostrand Reinhold, New York, 1945).
[46]E. S. Whitney, T. Haeber, M. D. Schuder, A. C. Blair, and D. J. Nesbitt, "High-resolution infrared studies in slit supersonic discharges: CH_2 stretch excitation of jet-cooled CH_2Cl radical," J. Chem. Phys. **125**, 054303 (2006).
[47]A. Kortyna, D. M. B. Lesko, and D. J. Nesbitt, "High-resolution sub-Doppler infrared spectroscopy of atmospherically relevant Criegee precursor CH_2I radicals: CH_2 stretch vibrations and "charge-sloshing" dynamics," J. Chem. Phys. **148**, 174308 (2018).
[48]A. B. McCoy, "The role of electrical anharmonicity in the association band in the water spectrum," J. Phys. Chem. B **118**, 8286–8294 (2014).
[49]S. Horvath, A. B. McCoy, B. M. Elliott, G. H. Weddle, J. R. Roscioli, and M. A. Johnson, "Anharmonicities and isotopic effects in the vibrational spectra of $X^-{\cdot}H_2O$, ·HDO, and $\cdot D_2O$ [X = Cl, Br, and I] binary complexes," J. Phys. Chem. A **114**, 1556–1568 (2010).
[50]A. B. McCoy, T. L. Guasco, C. M. Leavitt, S. G. Olesen, and M. A. Johnson, "Vibrational manifestations of strong non-Condon effects in the $H_3O^+{\cdot}X_3$ (X = Ar, N_2, CH_4, H_2O) complexes: A possible explanation for the intensity in the "association band" in the vibrational spectrum of water," Phys. Chem. Chem. Phys. **14**, 7205 (2012).
[51]J. R. Roscioli, E. G. Diken, M. A. Johnson, S. Horvath, and A. B. McCoy, "Prying apart a water molecule with anionic H-bonding: A comparative spectroscopic study of the $X^-{\cdot}H_2O$ (X = OH, O, F, Cl, and Br) binary complexes in the 600–3800 cm^{-1} region," J. Phys. Chem. A **110**, 4943–4952 (2006).
[52]M. C. Thompson and J. M. Weber, "Enhancement of infrared activity by moving electrons through bonds – The case of CO_2 anion and carboxylate," Chem. Phys. Lett. **683**, 586–590 (2017).
[53]J. M. Hollas and D. Phillips, *Jet Spectroscopy and Molecular Dynamics* (Springer Science & Business Media, 1994).
[54]D. J. Nesbitt and C. M. Lovejoy, "Rigid bender analysis of van der Waals complexes: The intermolecular bending potential of a hydrogen bond," J. Chem. Phys. **96**, 5712–5725 (1992).
[55]C. M. Lovejoy, M. D. Schuder, and D. J. Nesbitt, "Direct IR laser absorption spectroscopy of jet-cooled CO_2HF complexes: Analysis of the ν_1 HF stretch and a surprisingly low frequency ν_6 intermolecular CO_2 bend," J. Chem. Phys. **86**, 5337–5349 (1987).
[56]D. Zhao, K. D. Doney, and H. Linnartz, "High-resolution infrared spectra of vibrationally excited HC_4H in a supersonic hydrocarbon plasma jet," J. Mol. Spectrosc. **296**, 1–8 (2014).
[57]J.-U. Grabow, N. Heineking, and W. Stahl, "A molecular beam microwave Fourier transform (MB-MWFT) spectrometer with an electric discharge nozzle," Z. Naturforsch. **46**, 914–916 (1991).
[58]M. Nakajima, Q. Yue, J. Li, H. Guo, and Y. Endo, "An experimental and theoretical study on rotational constants of vibrationally excited CH_2OO," Chem. Phys. Lett. **621**, 129–133 (2015).
[59]M. E. Sanz, M. C. McCarthy, and P. Thaddeus, "Vibrational excitation and relaxation of five polyatomic molecules in an electrical discharge," J. Chem. Phys. **122**, 194319 (2005).
[60]G. W. Flynn, "Collision-induced energy flow between vibrational modes of small polyatomic molecules," Acc. Chem. Res. **14**, 334–341 (1981).
[61]M. Capitelli, *Nonequilibrium Vibrational Kinetics* (Springer, Berlin, Heidelberg, 1986).
[62]B. J. Orr and I. W. M. Smith, "Collision-induced vibrational energy transfer in small polyatomic molecules," J. Phys. Chem. **91**, 6106–6119 (1987).
[63]B.-C. Chang, M. L. Costen, A. J. Marr, G. Ritchie, G. E. Hall, and T. J. Sears, "Near-infrared spectroscopy of bromomethylene in a slit-jet expansion," J. Mol. Spectrosc. **202**, 131 (2000).